Available online at www.sciencedirect.com
ScienceDirect
Journal of Sound and Vibration 301 (2007) 909–926
JOURNAL OF SOUND AND VIBRATION
www.elsevier.com/locate/jsvi

# Modeling of nonlinear complex stiffness of dual-chamber pneumatic spring for precision vibration isolations

Jeung-Hoon Lee, Kwang-Joon Kim*

*Department of Mechanical Engineering, Center for Noise and Vibration Control, Korea Advanced Institute of Science and Technology, Science Town, Daejeon 305-701, Republic of Korea*

Received 2 January 2006; received in revised form 21 September 2006; accepted 28 October 2006
Available online 20 December 2006

**Abstract**

Dual-chamber pneumatic springs are widely in the vibration isolation systems for precision instruments such as optical devices or nano-scale equipments owing to their superior stiffness- and damping-characteristics. In order to facilitate their design optimization or active control, a more accurate mathematical model or complex stiffness is needed. So far nonlinearities have not been dealt with.

Experimental results we obtained rigorously for a dual-chamber pneumatic spring exhibit significantly amplitude dependent nonlinear behavior, which cannot be described by linear models in earlier researches. In this paper, an improvement for the complex stiffness model is presented by taking two major considerations. One is to consider the amplitude-dependent complex stiffness of diaphragm necessarily employed for prevention of air leakage. The other is to use a dynamic model for oscillating flow in capillary tube connecting the two pneumatic chambers instead of unidirectional flow model. The proposed nonlinear complex stiffness model, which reflects dependency on both frequency and excitation amplitude is shown to be very valid by comparison with the experimental measurements. Such an accurate nonlinear model for the dual-chamber pneumatic springs would contribute to more effective design or control of vibration isolation systems.


## 1. Introduction

The dual-chamber pneumatic springs have been used recently as a key component of for vibration isolation tables for precision equipments such as optical devices, nano-scale instruments, etc. Owing to the volumetric compressibility of air, the pneumatic springs can have a lower stiffness than conventional isolators such as coil- or rubber- springs. Capillary tubes across the dual-chambers are employed to obtain sufficient damping efficiently. As the environmental vibration regulations [1,2] for precision instruments become more stringent, it is required to improve further the isolation performance in a passive or active manner. In either case, more accurate modeling for the complex stiffness of the dual-chamber pneumatic springs is a most important prerequisite.

*Corresponding author. Tel.: +82 42 869 3024; fax: +82 42 869 8220.
*E-mail address:* kjkim@kaist.ac.kr (K.-J. Kim).

0022-460X/$ - see front matter © 2006 Elsevier Ltd. All rights reserved.
doi:10.1016/j.jsv.2006.10.029

**List of symbols**

| | |
|---|---|
| $f$, $F$ | force (N) |
| $A$ | area ($m^2$) |
| $x$ | dynamic amplitude (m) |
| $d$ | differential |
| $\Delta$ | difference |
| $p$, $P$ | pressure ($N/m^2$) |
| $V$ | volume ($m^3$) |
| $T$ | temperature (K) |
| $m$ | air mass in the chamber (kg) |
| $R$ | the universal gas constant ( = 286.9 (J/kg K)) |
| $e$ | internal energy (J/kg) |
| $h$ | enthalpy (J/kg) |
| $Q$ | heat transfer (J) |
| $W$ | work done (J) |
| $c_p(c_v)$ | the specific heat at constant pressure(volume) (J/K) |
| $\kappa$ | the specific heat ratio |
| $u$ | cross-sectional mean fluid velocity (m/s) |
| $\tau_w$ | wall shear stress ($N/m^2$) |
| $\rho$ | density ($kg/m^3$) |
| $\mu$ | dynamic viscosity ($N\,s/m^2$) |
| $t$ | time (s) |
| $K$ | minor loss coefficient |
| $fr$ | friction coefficient |
| $fr_o$ | friction coefficient for oscillating flow |
| $fr_u$ | friction coefficient for unidirectional flow |
| $\omega$ | excitation frequency (rad/s) |
| $Re$ | Reynolds number |
| $Re_\omega$ | kinetic Reynolds number |
| $A_0$ | dimensionless oscillation amplitude |
| F | Fourier transformation |
| $N$ | volume ratio |
| $k$ | stiffness (N/m) |

*Subscripts*

| | |
|---|---|
| $p$ | piston |
| 0 | static |
| exp | experiment |
| atm | atmosphere |
| $t$ | top chamber |
| $b$ | bottom chamber |
| $I$ | entrance (or inlet) to each chamber |
| $c$ | capillary tube |
| max | maximum |
| $s$ | single-chamber |
| $D$, $d$ | diaphragm, dual-chamber |

*Superscripts*

| | |
|---|---|
| • | first derivative with respect to time |
| - | cycle average |
| * | complex variable |

The schematic of a dual-chamber pneumatic spring is shown in Fig. 1, where a capillary tube connects the two pneumatic chambers. A rigid piston supports the payload including the isolation table and precision instruments. Additionally, a diaphragm or a rubber membrane of complicated shape is necessarily installed for prevention of air leakage. The two pneumatic chambers and capillary tube eventually act as a stiffness and a damping element, respectively. Basically, hence, the physical relations among the rigid-body dynamics of the piston, thermodynamics in the two pneumatic chambers and fluid dynamics across and in the capillary tube should be faithfully described together with the role of the diaphragm.

Shearer [3] suggested a nonlinear model for the pneumatic cylinder by considering thermodynamics in the chambers and unidirectional flow in the capillary tube. The mathematical formulations are quite difficult to deal with for a design or control purpose. Under the assumption of small piston movements, linear models were proposed by Harris et al. [4] and DeBra [5], who assumed without validation a linear relationship between the fluid velocity in the capillary tube and the pressure gradient across the tube. However, the linear model by Harris [4] and DeBra [5] showed discrepancies with the measured data to a significant extent.

A most recent research devoting to the improvement of modeling can be found in Erin and Wilson [6], who included the effects of the diaphragm to compensate for the observed disagreement. This was done by simply employing a linear dynamic model consisting of a viscous- and a hysteretic-damper and a spring for the diaphragm and by tuning the values for each of these parameters using experimental measurements.

Significantly amplitude-dependent dynamic behavior of a dual-chamber pneumatic spring was observed in our experimental measurements. With increase of the input level, real part of the measured complex stiffness shows a softening spring and the frequency where loss factor takes a maximum becomes lower. Thus, existing

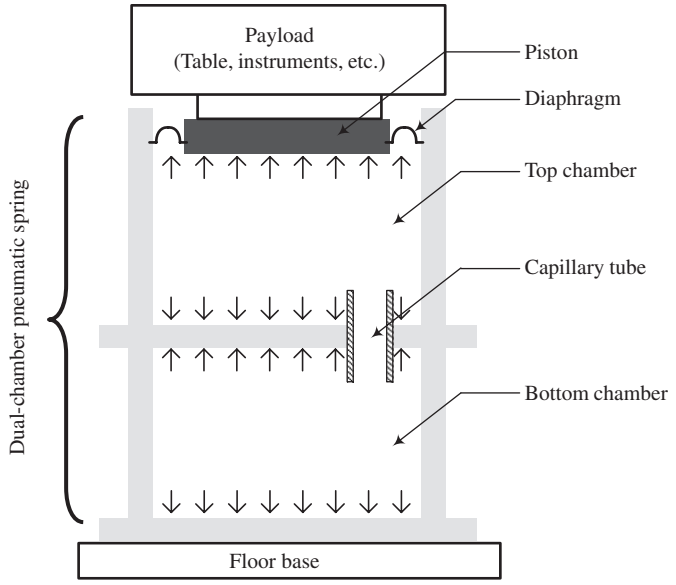


Fig. 1. Schematic of dual-chamber pneumatic spring with payload.

linear models [4–6] explained above are not adequate for the characteristics of amplitude dependent complex stiffness. An improvement for the nonlinear complex stiffness model was attempted in this paper.

First, complex stiffness of the diaphragm was obtained by subtracting the theoretical constant stiffness of the air from the measured complex stiffness of the pneumatic spring with single-chamber by blocking the capillary tube. This extraction yielded that the diaphragm stiffness is not only significant in its magnitude compared with the compressed air itself but also frequency as well as amplitude dependent. The softening stiffness of the diaphragm resembles very much to those of typical viscoelastic materials [7]. We included the amplitude dependent complex stiffness of the diaphragm in the modeling of the dual-chamber pneumatic spring. An argument on nonlinearity of the air itself inside chamber is also presented.

Second, another nonlinear behavior of the loss factor that the frequency where it peaks shifts to lower range with increase of the amplitude was observed. This was believed to be related with frictional characteristics of the air flow through capillary tube, since the capillary tube plays a key role of damping element in the dual-chamber pneumatic spring. In previous researches [4–6], theory of unidirectional flow, also known as Poiseuille flow [8], was employed to describe the air flow in capillary tube. The air in the capillary tube, in fact, is oscillating. Thus, in this paper, an oscillating flow theory [9,10] is employed to describe the fluid flow in capillary tube, where two similarity parameters instead of conventional Reynolds number is used to flow characterization.

Section 2 present experimental measurements on the complex stiffness, which motivated us to do this study. Development of an improved model and comparison with an existing model are presented in Section 3. Then, the improved complex stiffness model of the dual-chamber pneumatic spring will be validated with the experimental measurements.

## 2. Measurements of amplitude-dependent complex stiffness of dual-chamber pneumatic spring

An experimental apparatus for measurement of the complex stiffness is shown in Fig. 2, where the dual-chamber pneumatic spring (detail specifications in Table 1) with a static pressure $p_0$ was installed in a computer controlled servo-hydraulic actuation system, INSTRON dynamic material testing system (model: 8502). The displacement and force signals measured by a linear variable differential transformer (LVDT) and a load cell, respectively, are passed through signal conditioners and post-processed to attain the complex stiffness. Heavy line in Fig. 2 represents a pressurized line. A pressure gauge was installed to measure the applied pressure in the chamber, i.e. the pressure at static equilibrium, $p_0$. To investigate dependence on

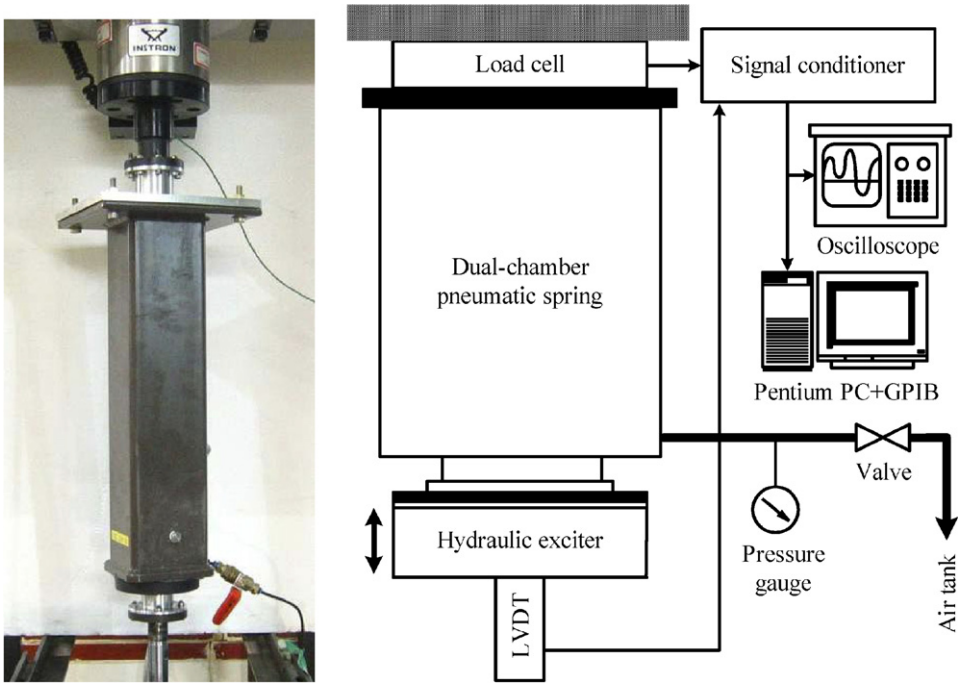


Fig. 2. Experimental set-up for complex stiffness measurement.

Table 1
Design specifications of employed pneumatic spring

| Symbol | Name | Value |
|---|---|---|
| $\rho$ | Density | $5.97\,\mathrm{kg/m^3}$ |
| $\mu$ | Dynamic viscosity | $1.79\times10^{-5}\,\mathrm{N\,s/m^2}$ |
| $R$ | Gas constant | $286.9\,\mathrm{J/kg\,K}$ |
| $\kappa$ | Specific heat ratio | 1.4 |
| $T_0$ | Temperature | 288.1 K |
| $P_0$ | Supplied pressure | $4.93\times10^5\,\mathrm{Pa}$ |
| $K$ | Minor pressure loss coefficient | 1.5 |
| $V_{t0}$ | Top chamber volume | $8.1\times10^{-4}\,\mathrm{m^3}$ |
| $V_{b0}$ | Bottom chamber volume | $1.5\times10^{-3}\,\mathrm{m^3}$ |
| $N$ | Volume ratio, $V_{b0}/V_{t0}$ | 1.9 |
| $L_c$ | Capillary tube length | $1.2\times10^{-2}\,\mathrm{m}$ |
| $D_c$ | Capillary tube diameter | $0.9\times10^{-3}\,\mathrm{m}$ |
| $A_p$ | Effective piston area | $5.3\times10^{-3}\,\mathrm{m^2}$ |

Table 2
Input conditions for the experiment: sinusoidal displacement excitation

| | |
|---|---|
| Dynamic amplitude (mm) | 0.05, 0.06, 0.07, 0.08, 0.09, 0.10, 0.15, 0.20, 0.30, 0.40, 0.50 |
| Frequency (Hz) | 0.2, 0.3, 0.4, 0.5, 0.6, 0.7, 0.8, 0.9, 1.0, 1.1, 1.2, 1.3, 1.4, 1.5, 1.6, 1.8, 2.0, 2.2, 2.4, 2.7, 3.0, 3.3, 3.7, 4.0, 5.0, 6.0, 7.0, 8.0, 9.0, 10.0, 12.0, 14.0, 16.0, 20.0, 24.0 |

dynamic amplitude and frequency for the dual-chamber pneumatic spring, sinusoidal displacement excitations (dynamic amplitude: 0.05–0.5 mm, driving frequency: 0.2–24 Hz, detailed in Table 2) were applied to the piston under a given preload corresponding to the weight of payload mass (100 kg).

Measurements of the complex stiffness of dual-chamber pneumatic spring are represented by solid lines in Fig. 3. Frequency- and amplitude-dependent stiffness and loss factor are visible at a first glance. Regarding the frequency dependence, real part of the complex stiffness, i.e., elastic stiffness increases slightly with frequency in low below about 1 Hz and high above about 10 Hz but increases dramatically in the mid-frequency ranges between 1 and 10 Hz. Loss factor, given by the imaginary part divided by real part of the complex stiffness and representing damping characteristics, shows bell-shaped curves in the frequency domain with the maximum values at frequency points where the real parts exhibit very rapid increase.

Amplitude-dependent behavior of the complex stiffness looks more complicated. The real part generally decreases with the amplitude. That is, softening stiffness characteristics [7] are observed. Furthermore, the frequency where the real parts show dramatic changes shift to the lower region. This seems to be quite relevant to the observation that the frequency of maximum loss factor moves from 4 to 1 Hz with increase of amplitude.

Thus, it is very clear that the complex stiffness of dual-chamber pneumatic spring has strong dependencies on the frequency as well as the dynamic amplitude. The linear models in previous researches [4–6] describe just frequency dependent behavior of the dual-chamber pneumatic spring without any mention on amplitude dependency. Therefore, a more accurate model of the dual-chamber pneumatic spring to include amplitude dependent characteristics is required.

An exploration to investigate the amplitude dependent behavior was performed by a single-chamber configuration, in which the capillary tube is blocked as depicted in Fig. 4. Dashed lines in Fig. 3 show measurements for the single-chamber configuration. The frequency dependence is simpler than that of the dual-chamber. That is, the real part increases with frequency slightly in a monotonous manner. The

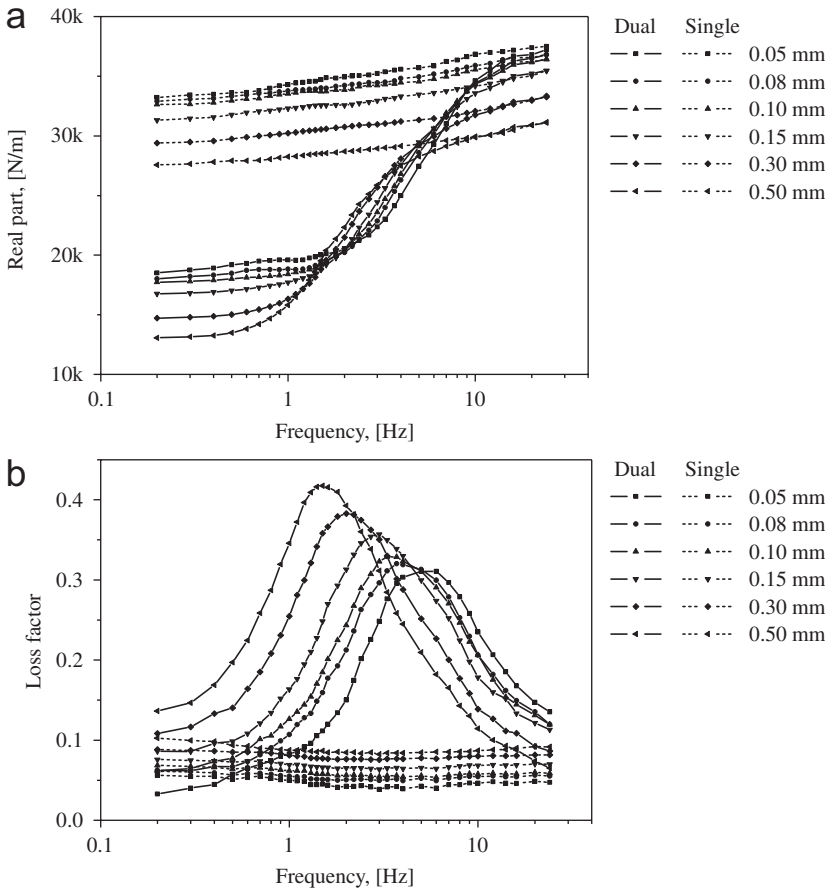


Fig. 3. Measured complex stiffness of pneumatic spring $k^*_{exp}$: (a) real part: Re[$k^*_{exp}$], (b) loss factor: Im[$k^*_{exp}$]/Re[$k^*_{exp}$].

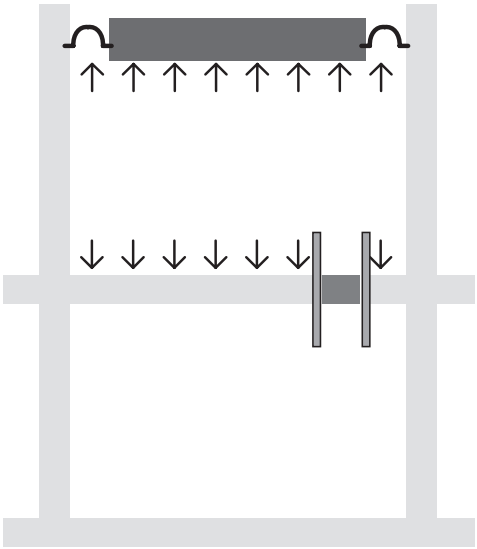

Fig. 4. Single-chamber configuration of pneumatic spring by blocking of capillary tube.

amplitude-dependent softening stiffness characteristics are almost the same as for the dual-chamber. It can be seen that the loss factor is not much frequency dependent but increases with the dynamic amplitude on the entire frequency ranges. Those observations are very similar to the typical characteristics of viscoelastic materials [7]. Since the effects of capillary tube were eliminated by the single-chamber configuration, the amplitude- and frequency-dependence represented by dashed lines in Fig. 3 can be considered to be due to the diaphragm made of rubber, which is a viscoelastic material under the assumption that the air behaves in a linear manner in the dynamic amplitude range although it may behave in a nonlinear manner for the static equilibrium. This thought means that the amplitude dependent complex stiffness of the diaphragm should be treated very carefully in modeling of the pneumatic spring.

It is to be noted in Fig. 3 that the measured complex stiffness of the dual- and single-chamber springs is nearly identical in the highest frequency range. This can be explained as follows. The air can move through the capillary tube in the lowest frequency range with negligible resistance. With increase of frequency, resistance of the air flow in the capillary tube increases. Then in the highest frequency range, the air flow gets blocked by the capillary tube. Such a frequency-dependent air flow in the capillary tube gives a change of effective volume along the frequency range. When blocking of air occurs, the pneumatic spring has a top-chamber volume only as its effective one. But the effective volume in the lowest frequency range is the sum of both top- and bottom-chamber one due to the negligible resistance of air flow. In other words, as graphically illustrated in Fig. 5, the dual-chamber pneumatic spring behaves like a single-chamber one of which the effective volume is the sum of those of both top- and bottom-chambers in the lowest frequency range, and another single-chamber one with only the top-chamber volume in the highest frequency range. Furthermore, it can be later known from Section 3 that the single-chamber type pneumatic spring without diaphragm does not have a damping characteristic, but a constant stiffness one with inversely proportional to the chamber volume. Therefore, the dual-chamber pneumatic spring has a hard stiffness in the high frequency range but a soft one in the low frequency range. At the same time, its damping characteristic (or loss factor) is significant only around mid-frequency ranges, where effective volume of dual-chamber pneumatic spring changes to top chamber from both top- and bottom-ones. Therefore, the highest frequency behavior of dual-chamber pneumatic spring is nearly identical to the single-chamber one with blocked capillary tube.

Another important observation on the loss factor measurements in Fig. 3(b) is that the frequency points of the maximum values move to the lower range with increase of vibration amplitudes. As explained above, the maximum loss factor is shown at the transition of effective volume. The increased level of vibration gives a more restriction on air flow across the capillary tube, which causes a transition of effective volume in the lower frequency ranges. In other words, by referring again Fig. 5, the frequency where dual-chamber pneumatic

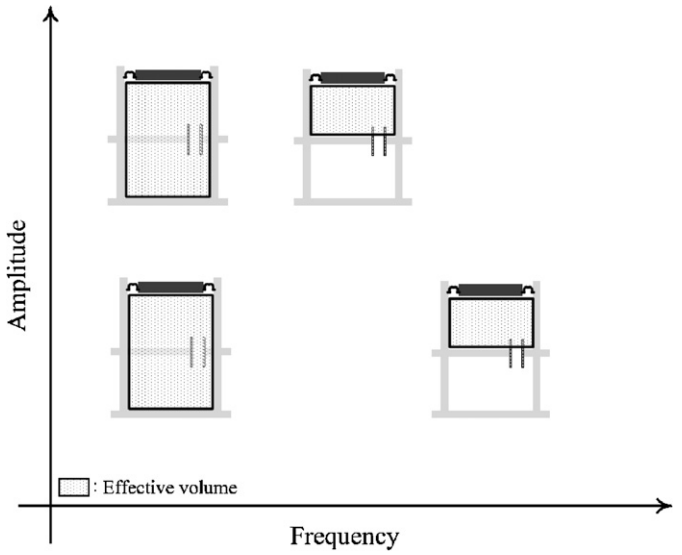


Fig. 5. Change of effective volume with respect to frequency and amplitude.

spring turns to be a single-chamber one with only the top-chamber volume moves to the lower frequency range along the vibration amplitude, since the increase of vibration amplitude results to the blocking of air in the lower frequency range. This means the frequency of maximum loss factor moves to the lower frequency range with increase of vibration amplitude. Thus, the observed nonlinear behavior of the air flow across capillary tube needs to be considered. In very limited input conditions of low amplitude and frequency, the flow in capillary tube would be almost steady one, which can be described by the linear unidirectional flow theory. But, for the case of higher input we concern, the actual flow would be close to the oscillating one, showing a nonlinear characteristic. Hence, in this study, an oscillating flow theory [9,10] is employed to reflect the nonlinear relation of air flow in capillary tube.

In summary, amplitude as well as frequency-dependent behavior of a dual-chamber pneumatic spring have been clearly pointed out. The causes of such nonlinear behaviors are believed to be related to the viscoelastic properties of the diaphragm as well as the characteristics of oscillating flow in the capillary tube. These two sources are studied in more detail in next section.

## 3. Modeling of dual-chamber pneumatic spring

### *3.1. Complex stiffness of dual-chamber pneumatic spring with complex stiffness of diaphragm excluded*

Consider a dual-chamber pneumatic spring shown in Fig. 6 to derive a dynamic model for its complex stiffness. Static equilibrium in Fig. 6(a) is determined by payload mass, atmospheric pressure and chamber pressure. In Fig. 6(b), small piston movements by dynamic forces will change mass, pressure, volume and temperature of the air in upper chamber, cause the air to flow through the capillary tube, and consequently change mass, pressure, temperature in bottom chamber. Hence, complex stiffness defined as the force for unit displacement of the piston is related to rigid-body dynamics of the piston, thermodynamics in the pneumatic chambers and fluid dynamics across the capillary tube. Effects of diaphragm to prevent leakage of the air will be considered in Section 3.2.

#### *3.1.1. Rigid-body dynamics of the piston*

In static equilibrium where pressure in both chambers is constant and the same, the force at piston $f_p$ is given by

$$f_p = A_p(p_0 - p_{\text{atm}}), \tag{1}$$

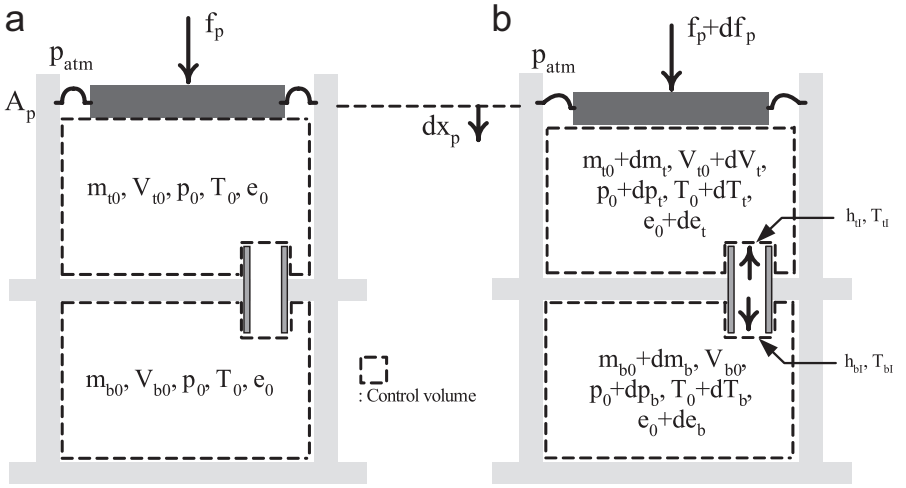


Fig. 6. Variables in static and dynamic equilibrium of dual-chamber pneumatic spring: (a) static equilibrium, (b) dynamic equilibrium.

where $p_0$ and $p_{\text{atm}}$ ( = 101.325 kPa) are absolute chamber pressure and atmospheric pressure, respectively, and $A_p$ an equivalent piston area to represent movement of both piston and diaphragm.

Dynamic displacement $\mathrm{d}x_p$ of the piston due to dynamic force $\mathrm{d}f_p$ on the piston causes pressure variations in top/bottom chambers, $\mathrm{d}p_t$ and $\mathrm{d}p_b$, respectively. The total force equilibrium is given by

$$f_p + \mathrm{d}f_p = A_p(p_0 + \mathrm{d}p_t - p_{\text{atm}}) \tag{2}$$

dynamic force is related to the pressure variation of top chamber by

$$\mathrm{d}f_p = A_p \mathrm{d}p_t, \tag{3}$$

$\mathrm{d}p_t$ need to be represented in terms of $\mathrm{d}x_p$ to derive the complex stiffness.

### 3.1.2. Thermodynamics of air in chambers

Dynamic displacement of the piston causes variations of mass ($m$), pressure ($p$), volume ($V$) and temperature ($T$) of the air in the chambers as depicted in Fig. 6, where subscripts '$t$' and '$b$' denote the top- and bottom chamber, respectively, '0' static equilibrium. The air in the chamber is assumed to be a perfect (or ideal) gas in both static- and dynamic-equilibrium state, respectively, as follows:

$$p_0 V_{i0} = m_{i0} R T_0 \quad (i = t, b), \tag{4}$$

$$(p_0 + \mathrm{d}p_i)(V_{i0} + \mathrm{d}V_i) = (m_{i0} + \mathrm{d}m_i)R(T_0 + \mathrm{d}T_i), \tag{5}$$

where $R$( = 286.9 J/(kg K)) denotes the universal gas constant. From Eqs. (4) and (5), a relationship between the rate of change in pressure, volume, mass and temperature can be derived as follows:

$$\frac{\dot{m}_i}{m_{i0}} = \frac{\dot{V}_i}{V_{i0}} + \frac{\dot{p}_i}{p_0} - \frac{\dot{T}_i}{T_0}, \tag{6}$$

where the rate of change of temperature $\dot{T}_i$ is determined by the type of thermal process in the chamber. The dual-chamber pneumatic spring actually results in neither an isothermal nor an adiabatic process, but polytropic. But for simplicity, two extreme cases, i.e., isothermal- and adiabatic-process are discussed in relation with the velocity of piston. In order to be an isothermal condition, the heat generated during the piston movement should not contribute to the variation of temperature, i.e., should be completely transferred to the environment. For such a heat transfer, the piston must have remarkably slow movements. In short, the isothermal process is a very slow process in a dynamical viewpoint. On the contrary, if the piston moves fast enough that all of the heat of the stroke is conserved, an adiabatic process occurs. Now it is important to

determine thermal process governing the pneumatic chamber, because the stiffness of pneumatic spring will change according to the thermal process. The polytropic constant, $n$, varies between the isothermal and adiabatic, i.e. $1<n<1.4$. Thus, the minimum stiffness occurs under an isothermal assumption, whereas the maximum stiffness an adiabatic one ($\sim$1.4 times of isothermal one). Based on approximate heat transfer calculations for the setup in this study, isothermal process is possible far below 0.1 Hz. In a rigorous sense, isothermal process can be possible only at DC (0 Hz). Thus, vibrations above 0.2 Hz in this study can be assumed as an adiabatic process. Although this assumption may cause a slight error in the prediction of stiffness characteristics, the polytropic process which actually governs pneumatic chamber is much closer to adiabatic than isothermal. Furthermore, adiabatic assumption is commonly accepted in the literature [4–6].

For an adiabatic process, the heat generated during a stroke does not escape the pneumatic chamber, but causes a variation of internal temperature. The first law of thermodynamics [11] can be employed for the description of temperature variation $\dot{T}_i$ in Eq. (6). That is to apply energy balance to each control volume and control surface depicted as dashed lines in Fig. 6 by using internal energy $e$ and enthalpy $h$. Once a static equilibrium state is reached, internal energy variations ($\mathrm{d}e_t, \mathrm{d}e_b$) due to the temperature changes are used to describe the dynamic equilibrium. Besides, enthalpy ($h_{tI}, h_{bI}$) and temperature ($T_{tI}, T_{bI}$) at control surface, i.e., at the entrance to each chamber are used to reflect the air flow across the capillary tube.

The first law of thermodynamics for the top chamber gives

$$\mathrm{d}Q - \mathrm{d}W = [-\mathrm{d}m_t h_{tI}]_{\mathrm{cs}} + [(m_{t0} + \mathrm{d}m_t)(e_0 + \mathrm{d}e_t) - m_{t0}e_0]_{\mathrm{cv}}, \tag{7}$$

where $\mathrm{d}Q$, heat exchange with the environment, becomes zero by the adiabatic process assumption. The work-done $\mathrm{d}W$ is given by $p_0 \mathrm{d}V_t$ under the small piston displacement. In the right-hand side of Eq. (7), the first- and second-part imply the energy balance at the control surface (cs) and control volume (cv), respectively. For an ideal gas, both enthalpy and internal energy depend solely on temperature [11] as follows:

$$h_{tI} = c_p T_{tI}, \tag{8}$$

$$e_0 = c_v T_0, \quad \mathrm{d}e_t = c_v \mathrm{d}T_t, \tag{9}$$

where $c_p$ and $c_v$ denote specific heat capacity at constant pressure and constant volume, respectively, and the specific heat ratio $\kappa$ defined as $c_p/c_v$ is 1.4 for the air. Using Eqs. (8) and (9) in Eq. (7) and dividing by the time variation $\mathrm{d}t$, the relation of temperature variation for top chamber can be readily derived:

$$m_{t0} c_v \dot{T}_t = (c_p T_{tI} - c_v T_0)\dot{m}_t - p_0 \dot{V}_t. \tag{10}$$

Similarly, that for bottom chamber is obtained as follows:

$$m_{b0} c_v \dot{T}_b = (c_p T_{bI} - c_v T_0)\dot{m}_b. \tag{11}$$

Further substitution of Eqs. (10) and (11) into Eq. (6) gives mass flow rate into each chamber, respectively:

$$\dot{m}_t = \frac{1}{RT_{tI}}\left[p_0 \dot{V}_t + \frac{V_{t0}}{\kappa}\dot{p}_t\right], \tag{12}$$

$$\dot{m}_b = \frac{1}{RT_{bI}}\left[\frac{V_{b0}}{\kappa}\dot{p}_b\right]. \tag{13}$$

In Eqs. (12) and (13), $T_{tI}$ and $T_{bI}$ representing temperature of the air at the ends of the capillary tube in the top- and bottom-chamber, respectively, are unknown without the knowledge of temperature distribution through the capillary tube, which is very difficult to estimate in an analytical way. According to Shearer [12], temperature variation in the capillary tube is negligible under small motions. This enables an assumption that $T_{tI}$ and $T_{bI}$ be identical to $T_0$, which allows Eqs. (12) and (13) to be in simpler forms:

$$\dot{m}_t = \frac{1}{RT_0}\left[p_0 \dot{V}_t + \frac{V_{t0}}{\kappa}\dot{p}_t\right], \tag{14}$$

$$\dot{m}_b = \frac{1}{RT_0}\left[\frac{V_{b0}}{\kappa}\dot{p}_b\right]. \tag{15}$$

*3.1.3. Fluid-dynamics for air flow in capillary tube*

The thermodynamic relations of pressure, volume, temperature in the top- and bottom-chamber treated separately in previous section are to be coupled with each other by the air flow rate in the capillary tube and the pressure difference across the capillary tube.

The momentum equation governing the air flow in the capillary tube can be derived by applying the Newton's 2nd law to a dotted differential fluid element in Fig. 7, where $x_c$ is the coordinate along the capillary tube, $u$ mean fluid velocity, $L_c$ and $A_c(D_c)$, respectively, length and cross-sectional area(diameter) of the circular capillary tube, $\tau_w$ wall shear stress due to the friction, and $p$ and $p+\mathrm{d}p$, respectively, the pressures across the differential element:

$$pA_c - (p+\mathrm{d}p)A_c - \tau_w(\pi D_c\,\mathrm{d}x_c) = \frac{\partial}{\partial t}(\rho u A_c)\,\mathrm{d}x_c + \rho u A_c(u+\mathrm{d}u) - \rho u A_c\,u. \tag{16}$$

Density of the air $\rho$ in the capillary tube may be actually time varying, since the air in the chambers undergoes compression or expansion. Compressibility of a gas can be neglected for a fluid-dynamic analysis if the Mach number of the flow is less than 0.3 [13]. The Mach number of the air flow in this study is about $10^{-3}$, which is far below 0.3. This allows the air in the capillary tube to be regarded as an incompressible fluid, reducing Eq. (16) the following:

$$-\frac{\mathrm{d}p}{\mathrm{d}x_c} = \rho\,\frac{\mathrm{d}u}{\mathrm{d}t} + \frac{4}{D_c}\tau_w. \tag{17}$$

If we further assume that the pressure gradient is constant along the capillary tube, i.e., $-\mathrm{d}p/\mathrm{d}x_c \approx (p_t - p_b)/L_c \equiv \Delta p/L_c$, and that the inertia term in the first part of right-hand side can be negligible, then the above equation can be reduced to Eq. (18):

$$\Delta p = \frac{4L_c}{D_c}\tau_w. \tag{18}$$

Here, the assumption of constant pressure gradient is well accepted to the fluid-mechanics researchers. Its experimental validation can be found Hagen's data [8], where he measured steady water flow in brass pipes and found linear relationship between pressure drop and fluid velocity. It may be difficult to assure that the assumption of constant pressure gradient does hold for our case, i.e., a fluctuating air. However, we decided to employ this assumption for a simple- and closed-form of momentum equation in the capillary tube. Otherwise computational fluid mechanics (CFD) techniques are required to solve the momentum equation, which is far beyond our research scope.

Substituting an expression for the wall shear stress $\tau_w$ represented by the product of dynamic pressure and friction coefficient $fr$ [8]:

$$\tau_w = \frac{\rho|u|u}{8}fr \tag{19}$$

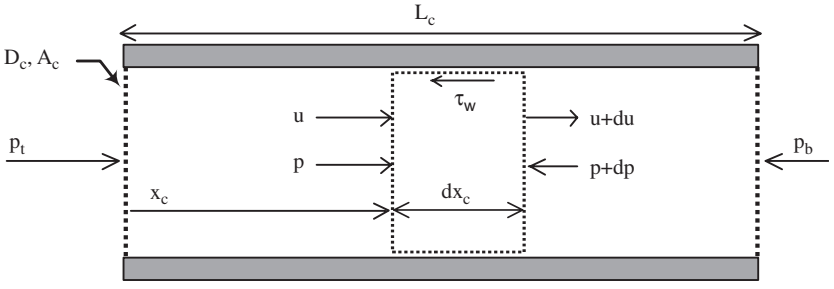


Fig. 7. Diagram for modeling of air flow in capillary tube.

into Eq. (18) and further consideration of minor pressure loss $K$ at the inlet and outlet of the capillary tube [8] results in Eq. (20):

$$\Delta p = \left(\frac{L_c}{D_c} fr + K\right) \frac{\rho}{2} |u| u. \tag{20}$$

For harmonic piston movements, the fluid velocity $u$ takes a harmonic function:

$$u = u_{\max} \sin \omega t. \tag{21}$$

Thus, the nonlinear term $|u|u$ in Eq. (20) can be linearized by the use of Fourier series 1st-order approximation as follows:

$$\begin{aligned} |u|u &\cong \left[\frac{\omega}{\pi}\int_0^{2\pi/\omega} |\sin \omega t| \sin^2 \omega t \, \mathrm{d}t\right] u_{\max}^2 \sin \omega t + \left[\frac{\omega}{\pi}\int_0^{2\pi/\omega} |\sin \omega t| \sin \omega t \cos \omega t \, \mathrm{d}t\right] u_{\max}^2 \cos \omega t \\ &= \frac{8 u_{\max}}{3\pi} u. \end{aligned} \tag{22}$$

The pressure difference across the capillary tube then can be finally formulated as follows:

$$\Delta p = \left(\frac{L_c}{D_c} fr + K\right) \frac{4\rho u_{\max}}{3\pi} u, \tag{23}$$

which shows that the pressure loss is approximated by the friction at the tube wall and minor loss at the inlet and outlet of capillary tube. The ratio of frictional loss $(L_c/D_c)fr$ to minor loss $K$ generally decreases with increase of the fluid velocity in the capillary tube, which means that minor loss become more important in the higher frequency range. In the frequency range of 2–5 Hz where the damping of capillary tube becomes important, the ratio is about 10 and, hence, damping due to frictional loss inside the capillary tube turns to be far more important than the one due to minor loss. Consideration of minor loss was not made in the linear flow model of previous researches [4–6], but it will be included in our case for a faithful description of nonlinear air flow.

If the flow in capillary tube is unidirectional, the friction coefficient $fr$ in Eq. (23) solely depends on a single similarity parameter, Reynolds number [8], and is quite well established in the classical fluid-dynamics. Noting that the actual flow in the capillary tube is oscillating, it was decided to employ a friction coefficient for oscillating flow.

The friction coefficient for an oscillating flow proposed by Zhao [9,10] and denoted by $fr_o$ replaces $fr$ in Eq. (23) will be called oscillating friction coefficient here. The oscillating friction coefficient $fr_o$ is dependent on two similarity parameters instead of one for the unidirectional friction coefficient $fr_u$. That is, $fr_o$ is given by a function of kinetic Reynolds number $Re_\omega (= \rho\omega D_c^2/\mu)$ and dimensionless oscillation amplitude $A_0 (= x_{\max}/D_c)$ for laminar and turbulent flows, respectively, as follows:

$$fr_o = \frac{4}{A_0}\left(\frac{3.27}{\mathrm{Re}_\omega^{0.548} - 2.04}\right) \quad \text{for} \quad 23 \leqslant \mathrm{Re}_\omega \leqslant 395 \quad \text{and} \quad 0 \leqslant A_0 \leqslant 26.4, \tag{24}$$

$$= \frac{4}{A_0}\left(\frac{76.6}{\mathrm{Re}_\omega^{1.2}} + 0.41\right) \quad \text{for} \quad 81 \leqslant \mathrm{Re}_\omega \leqslant 540 \quad \text{and} \quad 53.4 \leqslant A_0 \leqslant 113.5. \tag{25}$$

Here, $x_{\max} (= u_{\max}/\omega)$ denotes the amplitude of fluid displacement, and $\mu$ the coefficient of dynamic viscosity of air.

In previous researches [4–6], the air flow in the capillary tube was assumed to be not only unidirectional but also laminar one so that the model was constrained to be linear and, hence, not able to describe nonlinear behavior. A friction coefficient for unidirectional flows $fr_u$ known as Darcy friction factor depends only on Reynolds number $Re$ and given by

$$fr_u = \frac{64}{\mathrm{Re}} \quad \text{for} \quad \mathrm{Re} \leqslant 2300 \tag{26}$$

just for the laminar flow region, where the Reynolds number is defined as follows:

$$\mathrm{Re} = \frac{\rho \bar{u} D_c}{\mu}. \tag{27}$$

$\bar{u}$ in the above Eq. (27) denotes the cycle-averaged fluid velocity, i.e., computed by

$$\bar{u} = \frac{\omega}{2\pi} \int_0^{2\pi/\omega} |u| \, \mathrm{d}t = \frac{2}{\pi} u_{\max}. \tag{28}$$

The two different air flow models will be compared with measurements in terms of the complex stiffness for a dual-chamber pneumatic spring later in this paper.

*3.1.4. Combining three dynamic models*

One rigid-body dynamic Eq. (3) for the piston, two thermodynamic Eqs. (14) and (15) for the pneumatic chambers and one fluid dynamic Eq. (23) for the capillary tube, all of which described in time domain, can be combined to derive the complex stiffness of the whole system. For a given value of dynamic displacement $\mathrm{d}x_p$, 6 unknowns of $\mathrm{d}p_t$, $\mathrm{d}p_b$, $\mathrm{d}m_t$, $\mathrm{d}m_b$, $\mathrm{d}m_{tb}$ and $\mathrm{d}f_p$ in the above 4 equations can be solved for by introducing two more the so-called continuity relations for mass flow rates between chambers and capillary tube

$$\dot{m}_t = -\dot{m}_{tb}, \tag{29}$$

$$\dot{m}_{tb} = \dot{m}_b, \tag{30}$$

where $\dot{m}_{tb}$ denotes the mass flow rate in the capillary tube.

Fourier transformations, i.e. frequency domain representations of the above dynamic relations give the complex stiffness of dual-chamber pneumatic spring in the following. First, Eq. (3) is transformed into frequency domain:

$$\mathrm{d}F_p(\omega) = A_p \, \mathrm{d}P_t(\omega). \tag{31}$$

Knowing that volume variation of the top chamber is the product of equivalent piston area $A_p$ and displacement of piston $\mathrm{d}x_p$, the frequency domain representation of Eqs. (14) and (15) for mass flow rates yields the followings:

$$\mathscr{F}[\dot{m}_t] = \frac{1}{RT_0}\left[p_0 A_p \mathrm{j}\omega X_p(\omega) + \frac{V_{t0}}{n}\mathrm{j}\omega P_t(\omega)\right], \tag{32}$$

$$\mathscr{F}[\dot{m}_b] = \frac{1}{RT_0}\left[\frac{V_{b0}}{n} P_b(\omega)\right], \tag{33}$$

where $\mathscr{F}$ denotes the Fourier transformation.

The fluid-dynamic Eq. (23) for velocity of the air in the capillary tube can be written in frequency domain as follows:

$$U(\omega) = \frac{P_t(\omega) - P_b(\omega)}{\left(\dfrac{L_c}{D_c} fr + K\right)\dfrac{4\rho u_{\max}}{3\pi}}, \tag{34}$$

which multiplied by $\rho A_c$ yields the mass flow rate across the tube

$$\mathscr{F}[\dot{m}_{tb}] = \rho A_c U(\omega) = \frac{P_t(\omega) - P_b(\omega)}{C(X_p, \omega)}. \tag{35}$$

$C(X_p, \omega)$ in Eq. (35) defined as below represents damping characteristics of the capillary tube:

$$C(X_p, \omega) \equiv \left(\frac{L_c}{D_c} fr(X_p, \omega) + K\right)\frac{4u_{\max}(X_p, \omega)}{3\pi A_c}. \tag{36}$$

For oscillating flows, $C(X_p, \omega)$ and $fr(X_p, \omega)$ in the above Eq. (36) are simply replaced with $C_o(X_p, \omega)$ and $fr_o(X_p, \omega)$ respectively and $u_{\max}$ is given by the following approximate continuity relation between at piston

and capillary tube:

$$u_{\max} \cong (A_p/A_c)X_p\omega, \tag{37}$$

where effects of compressibility of the air in top chamber are neglected just for simplicity. But, it might be negligible under small piston movement coming up to the hundreds of micrometer.

Substitution of Eqs. (32) and (35) into Eq. (29), substitution of Eqs. (33) and (35) into Eq. (30), and combining these with Eq. (31) give the complex stiffness of pneumatic spring without diaphragm $k_d^*(X_p,\omega)$ as follows:

$$k_d^*(X_p,\omega) \equiv -\frac{\mathrm{d}F_p(\omega)}{\mathrm{d}X_p(\omega)} = k_s\frac{1+\dfrac{V_{b0}C(X_p,\omega)}{RT_0\kappa}\mathrm{j}\omega}{N+1+\dfrac{V_{b0}C(X_p,\omega)}{RT_0\kappa}\mathrm{j}\omega}, \tag{38}$$

where

$$N \equiv V_{b0}/V_{t0}, \tag{39}$$

$$k_s \equiv \kappa p_0 A_p^2/V_{t0} \tag{40}$$

denote the ratio of the bottom- to top-chamber volume and the stiffness of single top chamber, respectively. It is noted that the single-chamber pneumatic spring without diaphragm given in Eq. (40) does not have a damping characteristic, but has a linear elastic stiffness which does not depend on input amplitude $X_p$ or frequency $\omega$. Furthermore, as mentioned in Section 2, the constant stiffness in Eq. (40) is inversely proportional to the chamber volume.

For comparison with oscillating flow damping characterized by $C_o(X_p,\omega)$, a damping for unidirectional laminar flow in earlier studies is designated as $C_u$ and given by

$$C_u = \frac{128\mu L_c}{\pi\rho D_c^4}, \tag{41}$$

which does not include minor loss at the inlet and outlet of the capillary. It is noted that this damping $C_u$ is independent of the dynamic amplitude and frequency and is equivalent to the flow restriction constant $C_r$ in Erin and Wilson [6].

Depending on the type of modeling of flow in the capillary tube $C(X_p,\omega)$, the complex stiffness $k_d^*(X_p,\omega)$ is classified into two types: $k_{d,o}^*(X_p,\omega)$ for oscillating flow modeling by Zhao and $k_{d,u}^*(\omega)$ for conventional unidirectional one by Darcy. Note that the latter model $k_{d,u}^*(\omega)$ proposed in earlier researches [4,5] depends on the frequency only and cannot describe the amplitude-dependent characteristics of the pneumatic spring observed in our measurements.

### 3.2. Consideration of dynamic characteristics of diaphragm

The diaphragm shown in Fig. 1, which is essentially used in air spring for sealing purpose primarily, eventually works as a complex stiffness element together with the air in the pneumatic chamber by pressurization of the air inside the chambers [6]. Thus, effects of the diaphragm need to be treated carefully in the dynamic modeling of the dual-chamber pneumatic spring.

The diaphragm used in pneumatic springs has a little complicated shape in its cross-sectional view and is typically made of viscoelastic materials like rubber. Since it works as a complex stiffness element only as the air pressure is increased, it is not easy to estimate the complex stiffness of the diaphragm alone in both computational and experimental ways. This paper proposes an indirect method for extraction of the complex stiffness of the diaphragm.

The idea is to measure the complex stiffness of a single-chamber spring consisting of air and diaphragm, e.g. by blocking the capillary tube in dual-chamber pneumatic spring as shown in Fig. 4 and just to eliminate the constant stiffness of air $k_s$ from the measurement data under the assumption that the stiffness of the air alone is given by Eq. (40). The complex stiffness of the diaphragm $k_D^*(X_p,\omega)$ estimated in such a way is shown

in Fig. 8. Because the stiffness of air alone is simply a constant, the frequency- and dynamic amplitude-dependent behaviors obtained for the single-chamber configuration in Fig. 3 are solely attributed to the diaphragm. The real part or elastic stiffness shows softening spring phenomenon for the whole frequency range and the loss factor increases with respect to the dynamic amplitude. Dependence of the real part and loss factor on the frequency is not so strong probably because the frequency range investigated is rather small. These observations for the diaphragm complex stiffness are very similar to typical characteristics of viscoelastic materials [7]. Thus, the proposed technique to estimate the complex stiffness of the diaphragm is believed to be reasonable since it is made of a viscoelastic material, rubber. In this study, the numerical complex stiffness data for the diaphragm shown in Fig. 8 will be directly applied to predict the complex stiffness model of dual-chamber pneumatic spring.

The total complex stiffness of the dual-chamber pneumatic spring can be represented by the sum of the complex stiffness of dual-chamber pneumatic spring without the diaphragm $k_d^*(X_p,\omega)$ and the one of the diaphragm $k_D^*(X_p,\omega)$ as follows:

$$k_{d+D}^*(X_p,\omega) \equiv k_d^*(X_p,\omega) + k_D^*(X_p,\omega), \tag{42}$$

because these two springs are connected in parallel in the dual-chamber pneumatic spring as depicted in Fig. 9.

For clarity, the total stiffness of the dual-chamber pneumatic spring will be distinguished by $k_{d+D,o}^*(X_p,\omega)$ and $k_{d+D,u}^*(X_p,\omega)$ depending on whether the flow in the capillary tube is modeled as an oscillating or

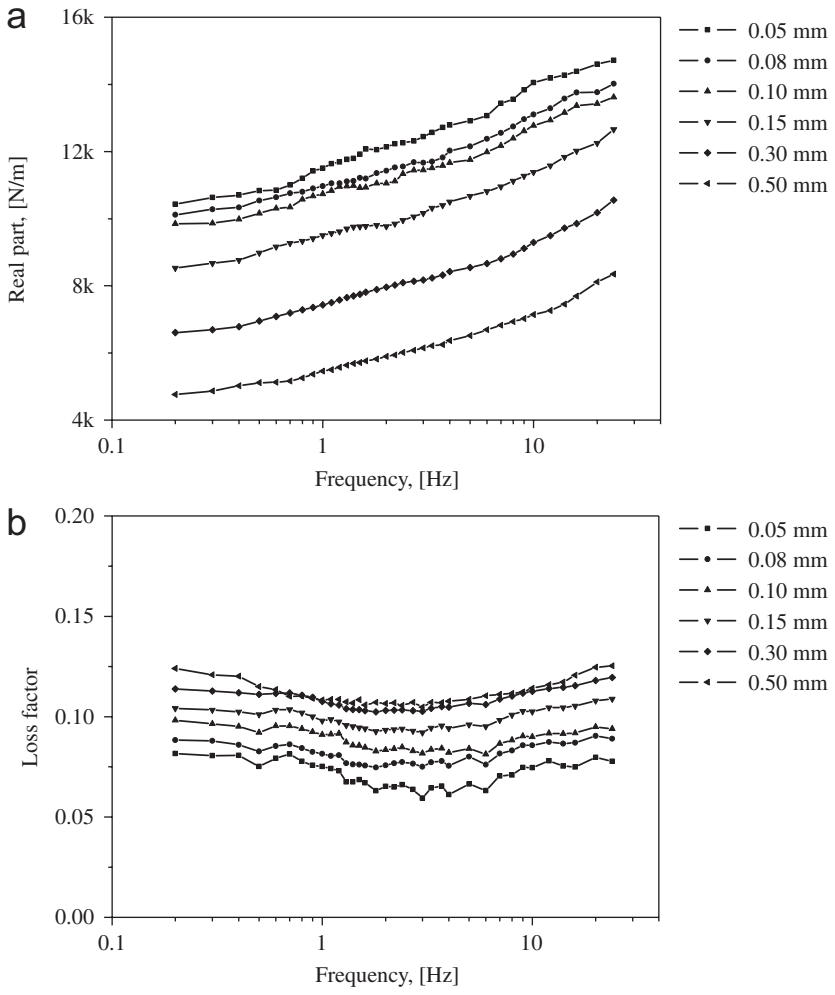


Fig. 8. Complex stiffness of diaphragm $k_D^*$: (a) real part: Re[$k_D^*$], (b) loss factor: Im[$k_D^*$]/Re[$k_D^*$].

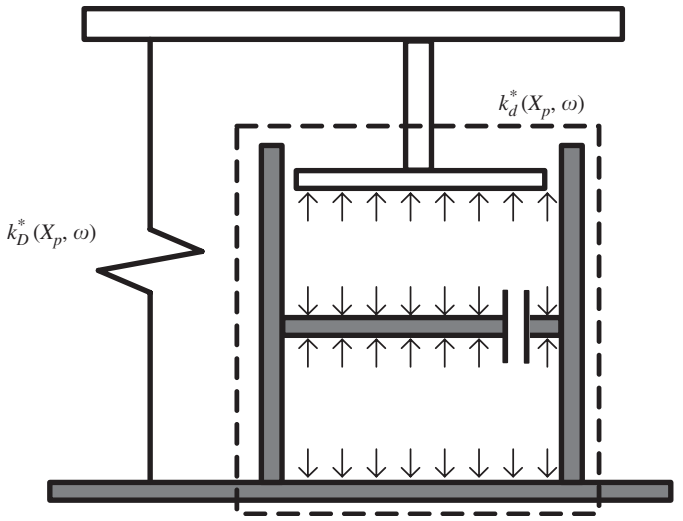


Fig. 9. Parallel connection of diaphragm stiffness with pneumatic spring stiffness.

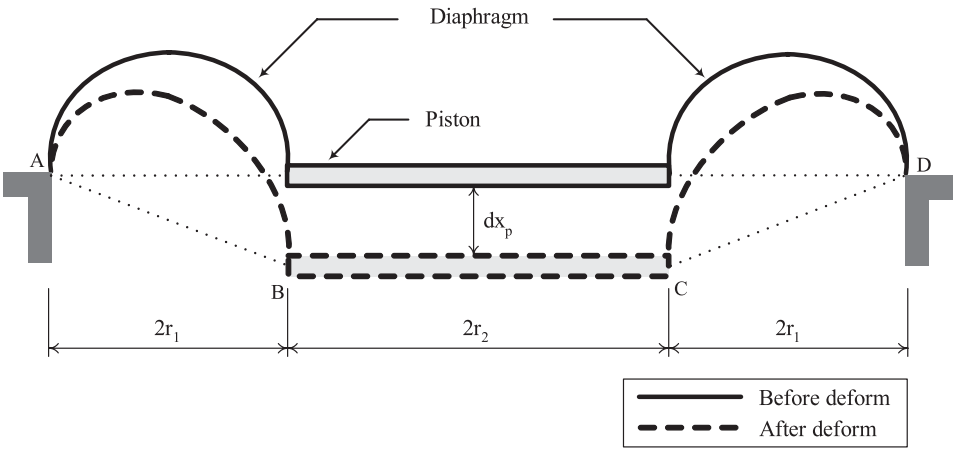


Fig. 10. Assumption of diaphragm movement for calculation of equivalent piston area $A_p$.

unidirectional. Due to the effects of diaphragm, $k^*_{d+D,u}(X_p, \omega)$ will have the dependency on not only frequency but also dynamic amplitude although $k^*_{d,u}(\omega)$ does not have a dependency on dynamic amplitude.

### 3.3. Comparison between predictions by the dynamic models and experimental measurements

The complex stiffness of dual-chamber pneumatic spring by the new dynamic model proposed in this paper is now compared with the one by the old model and experimental measurements. To compute the complex stiffness, the equivalent piston area $A_p$ in Eqs. (37), (40) and the minor pressure loss coefficient $K$ in Eq. (23) are required.

Fig. 10 shows deformation diagram of the diaphragm under the piston displacement of $\mathrm{d}x_p$ to obtain the equivalent piston area. Volume variation of the top chamber $\mathrm{d}V_t$ is approximated to be a part of a cone with cross-section ABCD as depicted in the figure. Thus, the equivalent piston area $A_p$ is obtained from dividing $\mathrm{d}V_t$ by $\mathrm{d}x_p$ as follows:

$$A_p = \mathrm{d}V_t/\mathrm{d}x_p = \pi(r_2^2 + 2r_2r_1 + 4r_1^2/3). \tag{43}$$

The minor pressure loss coefficient $K$ can be set as 0.5 and 1, respectively, at the sharp in-/out-let of a capillary tube between two large reservoirs [8]. Since the top- and bottom-chambers in the pneumatic chamber can be regarded as two large reservoirs, the value of $K$ in this study is chosen by the sum of these values 1.5. All parameter values are stated in Table 1 with physical dimensions of the pneumatic spring. Now, for the given input conditions at piston $X_p$ and $\omega$, the two complex stiffness $k^*_{d+D,o}(X_p,\omega)$ and $k^*_{d+D,u}(X_p,\omega)$ can be calculated by using the values listed in Table 1.

Comparison results between the experimental data and predictions by the complex stiffness models are shown in Fig. 11 for three levels of input magnitudes. The measurement data are quite well predicted by the newly proposed stiffness model $k^*_{d+D,o}(X_p,\omega)$ employing the oscillating flow in the capillary tube as well as amplitude dependent complex stiffness of the diaphragm. The average value of root mean square errors between predictions and measurements for various input levels are 2% and 8% for the real part and loss

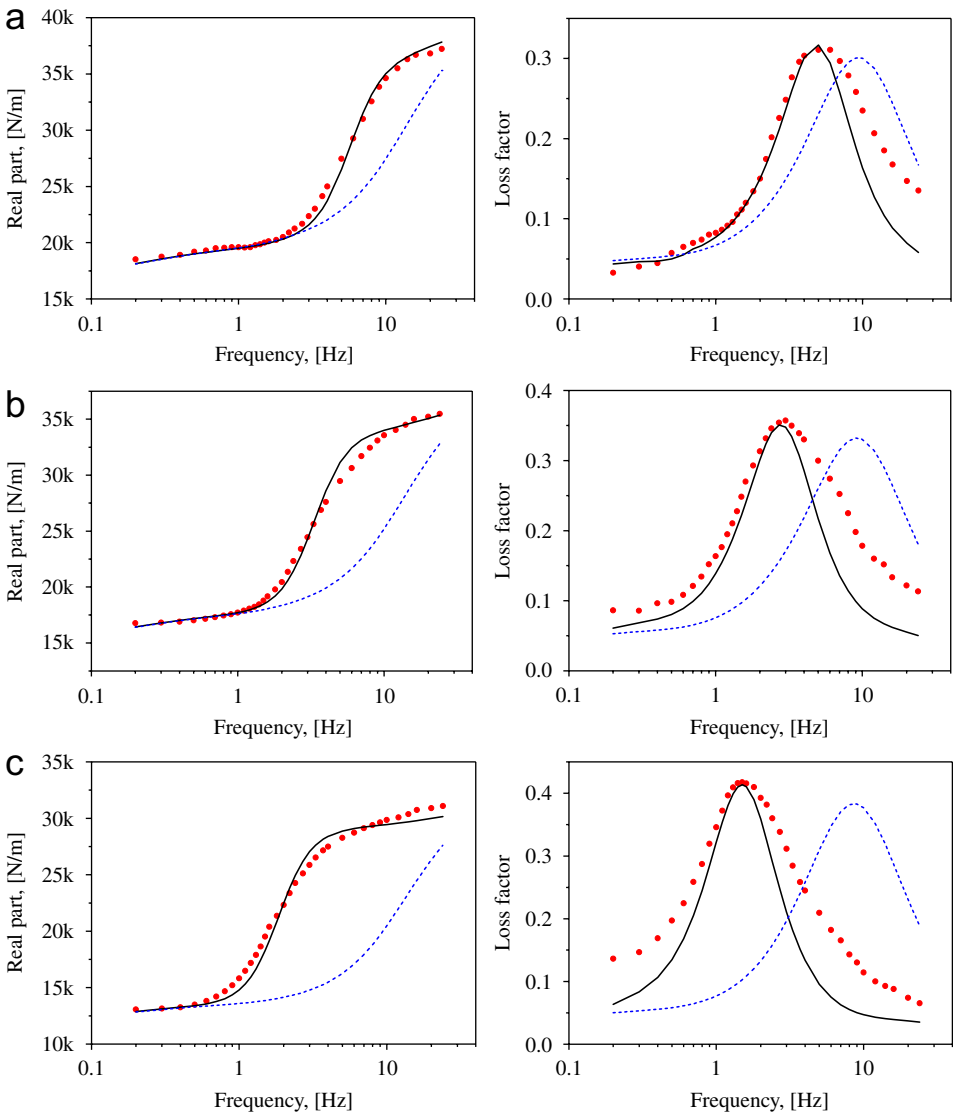


Fig. 11. Comparison between complex stiffness by models ($k^*_{d+D}$) and measurements ($k^*_{\exp}$): real part: Re[$k^*_{d+D}$] and Re[$k^*_{\exp}$], loss factor: Im[$k^*_{d+D}$]/Re[$k^*_{d+D}$] and Im[$k^*_{\exp}$]/Re[$k^*_{\exp}$]; ●, experiments; ———, $k^*_{d+D,o}$; - - - - -, $k^*_{d+D,u}$: (a) dynamic amplitude: 0.05 mm, (b) dynamic amplitude: 0.15 mm, (c) dynamic amplitude: 0.5 mm.

factor, respectively. It is noted that, as the dynamic amplitude increases, the discrepancies for the loss factor increases in the low- and high-frequency ranges, i.e., at frequencies off the peak points. Yet, the new complex stiffness model $k^*_{d+D,o}(X_p,\omega)$ predicts well the nonlinear behaviors of the dual-chamber pneumatic spring that we primarily concern. In more detail, inclusion of the amplitude-dependent complex stiffness of the diaphragm gives a very good prediction of softening of the elastic stiffness and increment of maximum loss factor for the whole pneumatic spring as the input level is increased. Furthermore, modeling by the oscillating flow of the one in the capillary tube represents fairly well shifting of the frequency where the loss factor takes it maximum and the slope of the elastic stiffness is steepest.

It can be seen in Fig. 11 that discrepancies between the experimental measurements and predictions by the conventional complex stiffness model $k^*_{d+D,u}(X_p,\omega)$ employing the unidirectional flow increase significantly as the input conditions, i.e., dynamic amplitude and/or frequency change. Closeness between the new stiffness model $k^*_{d+D,o}(X_p,\omega)$ and the conventional model $k^*_{d+D,u}(X_p,\omega)$ in the lower dynamic amplitude and/or frequency ranges points out an observation that frictional characteristics of the flow in the capillary tube predicted by the unidirectional flow model can represent those for the actual oscillating flow only under very limited input conditions of low amplitude and frequency. In order to include higher-level input conditions, modeling by the oscillating flow is definitely required. Furthermore, if the amplitude dependent complex stiffness of the diaphragm were not included in the conventional stiffness modeling $k^*_{d+D,u}(X_p,\omega)$ as in this study, softening behavior of the elastic stiffness and increase of the maximum value of loss factor could not be represented as shown in Fig. 11.

## 4. Concluding remarks

Nonlinear behaviors of a dual-chamber pneumatic spring were observed through careful experiments. In order to be able to describe the observed nonlinear behaviors, conventional linear complex stiffness model was improved by reflecting characteristics of oscillating flow in the capillary tube and amplitude-dependent complex stiffness of the diaphragm.

To this end, three relations: rigid-body dynamic of the piston, thermodynamics in the pneumatic chamber and fluid mechanics in and across the capillary tube were combined to obtain a resultant complex stiffness by including nonlinear characteristics of the diaphragm. Besides, two frictional flow models of oscillating and unidirectional flow were considered together for comparison. The new complex stiffness model of the dual-chamber pneumatic spring with nonlinear properties of the oscillating flow and viscoelastic diaphragm reflected in is proved to be very valid based on comparison with experimental measurements.

## Acknowledgments

This work has been supported financially by the Center for Nanoscale Mechatronics and Manufacturing of Korea Institute of Machinery and Materials (KIMM).

## References

[1] C.G. Gordon, Generic criteria for vibration-sensitive equipment, *Proceedings of SPIE*, San Jose, CA, 1991.
[2] H. Amick, M. Gendreau, C.G. Gordon, Facility vibration issues for nanotechnology research, *Proceedings of the Symposium on Nano Device Technology*, Hsinchu, Taiwan, 2002.
[3] J.L. Shearer, Study of pneumatic processes in continuous control of motion with compressed air, *Transactions of ASME* 78 (1956) 233–242.
[4] C.M. Harris, C.E. Crede, *Shock and Vibration Handbook*, McGraw-Hill, New York, 1961.
[5] D.B. DeBra, Design of laminar flow restrictors for damping pneumatic vibration isolators, *CIRP Annals* 33 (1) (1984) 351–356.
[6] C. Erin, B. Wilson, J. Zapfe, An improved model of a pneumatic vibration isolator: theory and experiment, *Journal of Sound and Vibration* 218 (1) (1998) 81–101.
[7] A.D. Nashif, D.I.G. Jones, J.P. Henderson, *Vibration Damping*, Wiley, New York, 1986.
[8] F.M. White, *Fluid Mechanics*, fifth ed., McGraw-Hill, New York, 2003.
[9] T.S. Zhao, P. Cheng, The friction coefficient of a fully-developed laminar reciprocating flow in a circular pipe, *International Journal of Heat and Fluid Flow* 17 (2) (1996) 167–172.

[10] T.S. Zhao, P. Cheng, Experimental studies on the onset of turbulence and frictional Losses in an oscillatory turbulent pipe flow, *International Journal of Heat and Fluid Flow* 17 (4) (1996) 356–362.
[11] Y.A. Cengel, M.A. Boles, *Thermodynamics: An Engineering Approach*, third ed., McGraw-Hill, New York, 1998.
[12] J.L. Shearer, *Fluid Power Control: Chapter 16 Pneumatic Drives*, MIT press, USA, 1960.
[13] P.H. Oosthuizen, W.E. Carscallen, *Compressible Fluid Flow*, McGraw-Hill, New York, 1997.